Synthesis of NiMn$_2$O$_4$/PANI Nanosized Composite with Increased Specific Capacitance for Energy Storage Application

Muhammad Abdullah [a], Syed Imran Abbas Shah [b], Karam Jabbour [c], Peter John [a], Muhammad Fahad Ehsan [d], Abdulnasser M. Karami [e], Muhammad Naeem Ashiq [b,*], Suleyman I. Allakhverdiev [f,g,*]

[a] Department of Chemistry, Government College University Lahore, Lahore-54000, Pakistan

[b] Institute of Chemical Sciences, Bahauddin Zakariya University, Multan-60800, Pakistan

[c] College of Engineering and Technology, American University of the Middle East, Egaila-54200, Kuwait

[d] Department of Civil and Environmental Engineering, Northeastern University, Boston 02115 MA USA

[e] Department of Chemistry, College of Science, King Saud University, Riyadh 11451, Saudi Arabia

[f] Controlled Photobiosynthesis Laboratory, K.A. Timiryazev Institute of Plant Physiology RAS, Botanicheskaya Street 35, Moscow, 127276 Russia

[g] Faculty of Engineering and Natural Sciences, Bahçeşehir University, Istanbul 34349, Türkiye

*= Corresponding authors,

E-mails: naeembzu@bzu.edu.pk (MNA); suleyman.allakhverdiev@gmail.com (SIA)

Stability analysis

The enduring stability of $NiMn_2O_4$/PANI was scrutinized through chronoamperometry (CA), contrasting its performance with that of RuO_2, as presented in Figure S1 (a). Results exhibited that $NiMn_2O_4$/PANI displayed superior stability over 50 h compared to RuO_2, a benchmark material. Cyclic constancy of $NiMn_2O_4$/PANI was further assessed *via* cyclic voltammetry (CV) at a sweeping rate of 5 mV s^{-1} over 10,000 cycles. Findings revealed remarkable stability of $NiMn_2O_4$/PANI, displaying minimal deviation in current density due to effective intercalation of electrolyte ions at electrode material interfaces. Figure S1 (b) depicted that $NiMn_2O_4$/PANI nanocomposite retained 96.58% of its capacitance after 5000 cycles and maintained a 93.61% rate capability after 10,000 stability cycles, as indicated in Figure S1 (c). These results suggest that the combined action of polyaniline and divalent nickel ions, alongside diverse morphology of nanocomposite, contributes to observed enhanced cycle stability. Microstructural irregularity of nanocomposites facilitates efficient charge transfer across polyaniline chains, that lead towards an increase in Cs and cycle stability. Polyaniline plays a crucial role in stabilizing $NiMn_2O_4$/PANI by providing a structured environment for nickel insertion-extraction responses, improving electrical conduction, and aiding the migration of charge carriers [1]. However, with repeated expansions and contractions, PANI chains gradually wear down, leading to an overall decrease in capacitance. To validate structural and morphological stability of the composite material post-stability characterization was conducted. Figure S1 (d) indicated that $NiMn_2O_4$/PANI maintained its structural integrity, showing no change in the 2θ degree values, consistent with the pre-stability XRD analysis. These results affirm sustained stability and structural robustness of $NiMn_2O_4$/PANI composite even after prolonged stability tests.
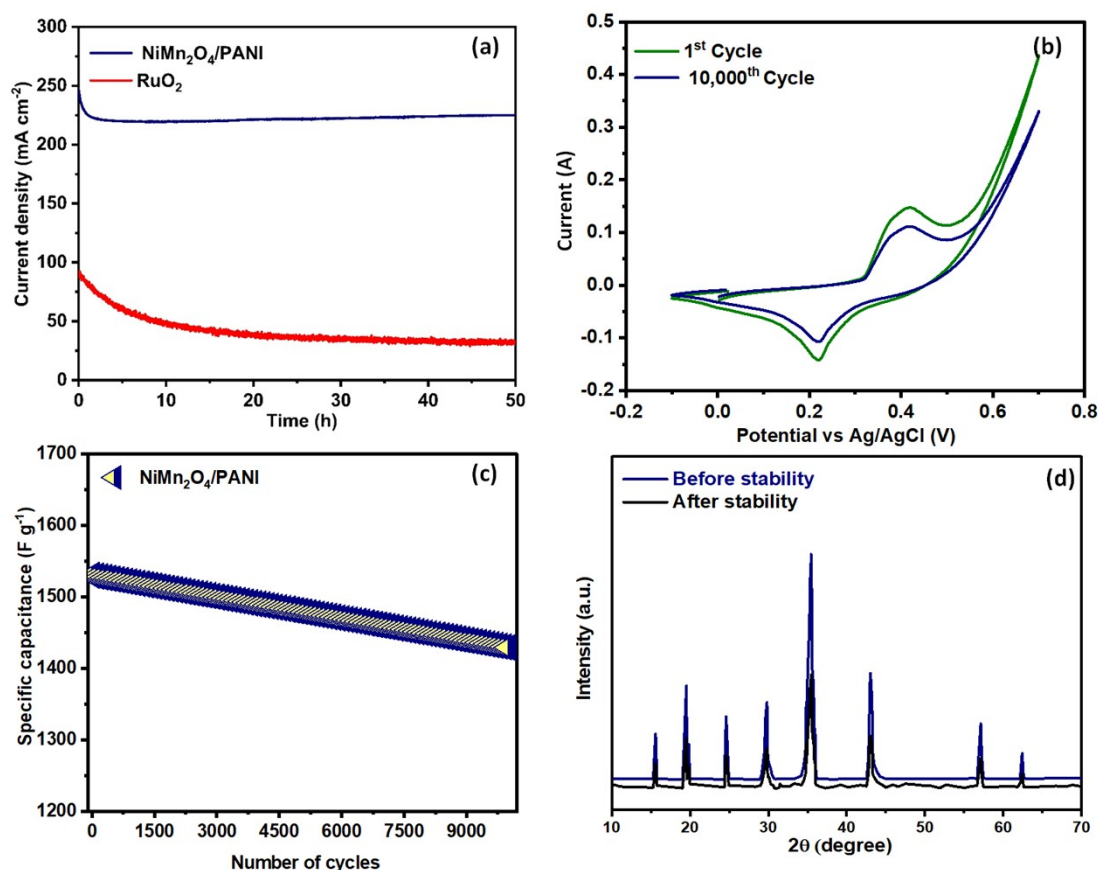
Figure S1: (a) Chronoamperometry, (b) CV stability cycle, (c) GCD stability cycle, and (d) XRD stability diffractogram of $NiMn_2O_4$/PANI.

The changes in the valence states of the $NiMn_2O_4$/PANI nanohybrid materials were investigated using XPS analysis. Analysis revealed elemental peaks for C 1s, O 1s, N 1s, Mn 2p, and Ni 2p, as illustrated in Figure S2 (a). Notably, there was an increase in intensity of O, signifying a higher concentration of oxygen-containing species, such as hydroxyl groups, in material after its use. Figure S2 (b) showed an increased intensity of C-O peaks, indicating an elevated presence of carbon-oxygen compounds in comparison to pre-stability carbonaceous materials. Conversely, the N 1s peaks exhibited a decrease after stability test, suggesting a reduction in nitrogen content, as depicted in Figure S2 (c). Moreover, the O 1s spectra presented a higher intensity in peaks related to OM-O and OO-H, indicating an increase in oxygen-containing species at electrode material interfaces, as demonstrated in Figure S2 (d). The Mn 2p XPS spectra showed a higher

intensity of Mn^{3+} species after stability testing compared to Mn^{2+}, indicating a conversion from Mn^{2+} to Mn^{3+}, as demonstrated in Figure S2 (e). Additionally, Figure S2 (f) presented two oxidation states after stability test, Ni^{2+} and Ni^{3+}, revealing that Ni^{2+} was oxidized to Ni^{3+}. These changes observed in the XPS spectra after stability testing indicate alterations in valence states of constituent elements in $NiMn_2O_4$/PANI nanocomposite. Transformation of oxidation states may significantly impact electrochemical behaviour of material and its subsequent performance in supercapacitor applications.
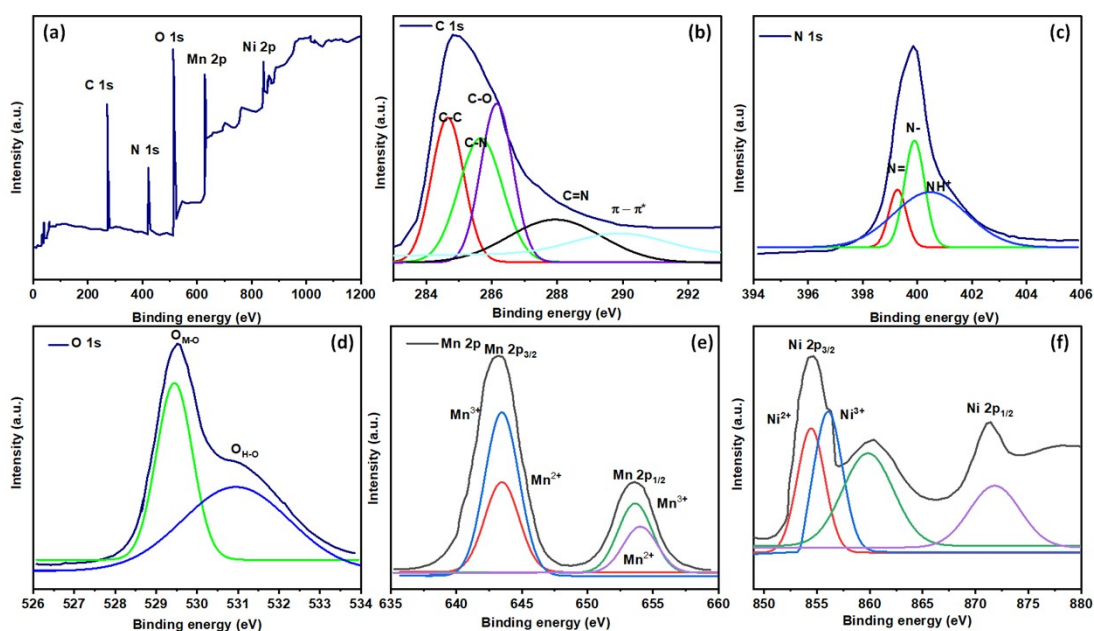

Figure S2. XPS spectra after stability of (a) full width scan (b) carbon 1s, (c) N 1s, (d) O 1s, (e) Mn 2p, and (f) nickel.

The post-stability surface analysis of recycled electrode material was conducted using SEM at a scale of 1 μm. Obtained results showcased nearly identical morphologies in oxidized materials after durability analysis, indicating stable behaviour of the fabricated materials, as depicted in Figure S3. These post-characterization assessments confirmed structural and morphological stability of material after undergoing 10,000 CV cycles and enduring 50 h of chronoamperometric studies. This consistent surface morphology post-testing suggests

robustness and resilience of material against the challenging electrochemical conditions, reaffirming its potential for prolonged and stable performance in supercapacitor applications.
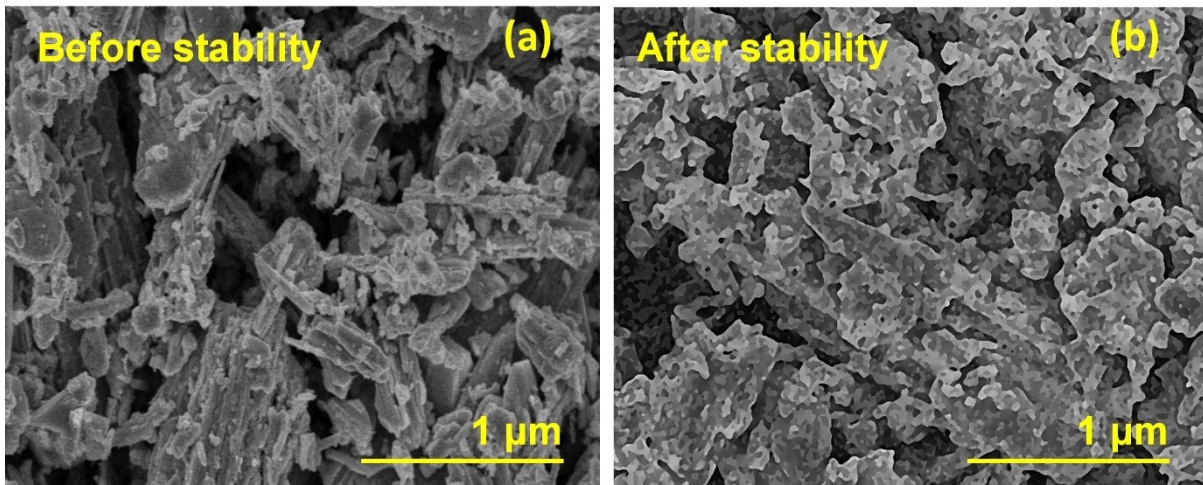

Figure S3. (a) Before stability and (b) after stability of $NiMn_2O_4$/PANI at 1 μm.

Assessing the self-discharge properties and leakage current of solid supercapacitors, often overlooked in recent studies, is imperative for the practical application of charge storage devices [2,3]. The device was charged to 1.0 V at 2 mA and then held at 1.0 V for 2 h to record leakage current data. In Figure S4 (a), it is observed that leaking current dropped significantly within the initial 15 min before stabilizing. Data collected indicates a minimal change in leakage current due to presence of the $NiMn_2O_4$/PANI nanocomposite. An open-circuit voltage versus time self-discharge test illustrates the reliability of stable supercapacitors. After reaching a 1.0 V charge for 20 min, as shown in Figure S4 (b), solid supercapacitors underwent a rapid self-discharge process within a few minutes, eventually stabilizing at an output voltage of 0.39 V after 20 h. All these results indicate that solid supercapacitors used in this study shows very low self-discharge rates, addressing a significant issue in practical electrical applications.
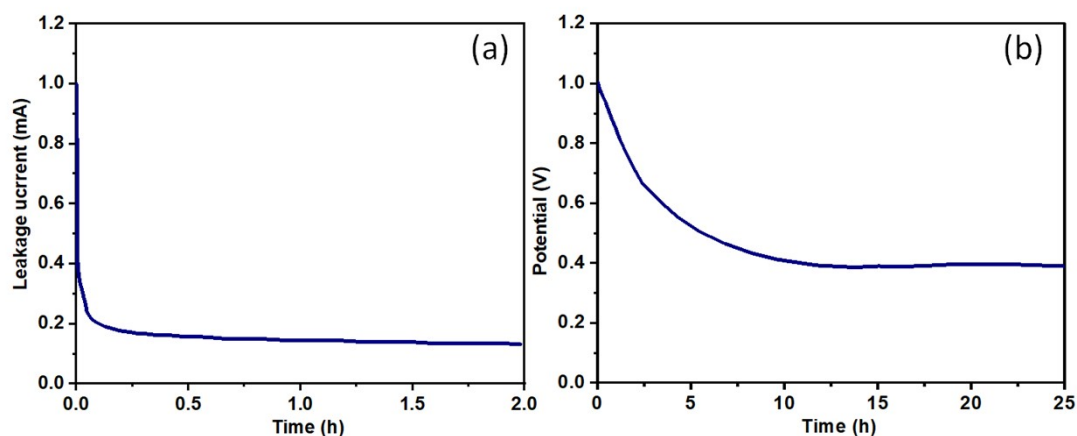
Figure S4. (a) Current leakage and (b) self-discharge characteristics of $NiMn_2O_4$/PANI nanocomposite.

Table S1: Comparison of specific capacitance (C_s) among fabricated nanohybrid material with another similar type of materials already reported.

Sr. No.	Materials	C_s (F g⁻¹)	Current density (A g⁻¹)	Electrolyte	Reference
1	$FeCo_2O_4$/PANI	940	1	1 M KOH	[4]
2	$GO/ZnFe_2O_4$/PANI	2169.71	1	1 M H_2SO_4	[5]
3	$NiCo_2O_4$/PANI	887	0.5	6 M KOH	[6]
4	$NiCo_2S_4$/PANI/CNT	1290	2	1 M KOH	[7]
5	$GO/CuCo_2O_4$/PANI	741.39	1	1 M KOH	[8]
6	$NiFe_2O_4$/PANI	448	1	1 M H_2SO_4	[9]
7	$CuCo_2O_4$/PANI	659	0.5	6 M KOH	[10]
8	$CdMn_2O_4$/PANI	210	1	1 M	[11]

				Na$_2$SO$_4$	
9	NiCo$_2$O$_4$/PANI	439.4	5	0.5 M H$_2$SO$_4$	[12]
10	rGO/NiMn$_2$O$_4$/PANI	757	1	1 M Na$_2$SO$_4$	[13]
11	**NiMn$_2$O$_4$/PANI**	**1530.01 ± 2**	**1**	**2 M KOH**	**Present work**

Reproducibility and Error Determinations:

Three cycles were performed on new electrodes with same mass loading and surface area, at 1 A/g current density in 2.0 M KOH, which yielded specific capacitance of 1530, 1528 and 1531 F/g. This data can be effectively used to determine experimental error with Csp of 1527 ±2. Upper threshold of +1 F/g and lower threshold of -2 F/g can be expected during the reproduction of similar electrode.
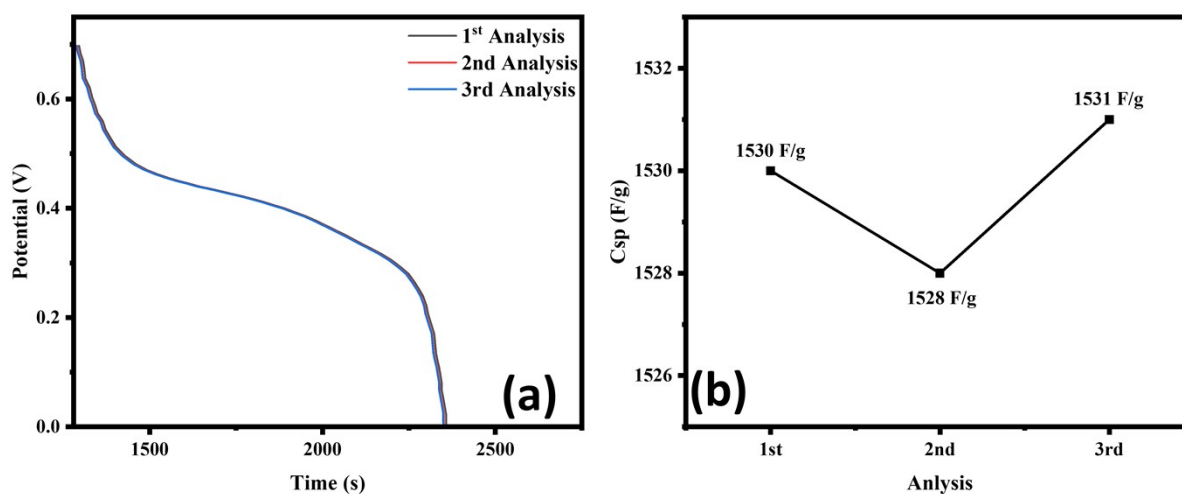
Figure S5. GCD error determination (a) GCD discharge cycles up to 3, and (b) Csp determined from these three cycles, at 1 A/g in 2.0 M KOH

Reference

1   F. Lyu, Y. Bai, Z. Li, W. Xu, Q. Wang, J. Mao, L. Wang, X. Zhang, Y. Yin, F. Lyu, Q. Wang, L. Wang, X. Zhang, Y. Bai, Z. Li, W. Xu, Y. Yin and J. Mao, *Adv. Funct. Mater.*, 2017, **27**, 1702324.

2   J. Zhou, L. Yu, W. Liu, X. Zhang, W. Mu, X. Du, Z. Zhang and Y. Deng, *Sci. Reports 2015 51*, 2015, **5**, 1–9.

3   C. Meng, C. Liu, L. Chen, C. Hu and S. Fan, *Nano Lett.*, 2010, **10**, 4025–4031.

4   S. Rajkumar, E. Elanthamilan, J. Princy Merlin and A. Sathiyan, *J. Alloys Compd.*, 2021, **874**, 159876.

5   Q. A. Alsulami, L. M. Alharbi, S. MAS Keshk, C. A. Qana Alsulami and N. and, *Int. J. Energy Res.*, 2022, **46**, 2438–2445.

6   V. Shanmugavalli and K. Vishista, *Mater. Res. Express*, , DOI:10.1088/2053-1591/AAE8EE.

7   X. Cheng, D. Wang, H. Ke, Y. Li, Y. Cai and Q. Wei, *Compos. Commun.*, 2022, **30**, 101073.

8   S. Verma, V. K. Pandey and B. Verma, *Synth. Met.*, 2022, **286**, 117036.

9   B. Senthilkumar, K. Vijaya Sankar, C. Sanjeeviraja and R. Kalai Selvan, *J. Alloys Compd.*, 2013, **553**, 350–357.

10   V. Shanmugavalli and K. Vishista, *J. Inorg. Organomet. Polym. Mater.*, 2020, **30**, 1448–1462.

11   J. Bhagwan, A. Sahoo, K. L. Yadav and Y. Sharma, *J. Alloys Compd.*, 2017, **703**, 86–95.

12   H. Xu, J. X. Wu, Y. Chen, J. L. Zhang and B. Q. Zhang, *Ionics (Kiel).*, 2015, **21**, 2615–2622.

13   S. Sahoo, S. Zhang and J. J. Shim, *Electrochim. Acta*, 2016, **216**, 386–396.